Rotational structures in ^{196}Hg

J. J. Lawrie,[1,*] E. A. Lawrie,[1,2] B. Msezane,[1,3] M. Benatar,[1,4] M. Fedderke,[1,4,†] G. K. Mabala,[1,4] S. Mukherjee,[1,‡] S. M. Mullins,[1] K. P. Mutshena,[1,§] N. J. Ncapayi,[1,2] R. T. Newman,[1,¶] J. F. Sharpey-Schafer,[1] F. D. Smit,[1] and P. Vymers[1,2]

[1]*iThemba LABS, National Accelerator Centre, P.O. Box 722, Somerset West 7129, South Africa*

[2]*Physics Department, University of the Western Cape, Private Bag X17, Bellville 7535, South Africa*

[3]*Physics Department, University of Zululand, Private Bag X1001, KwaDlangezwa 3886, South Africa*

[4]*Physics Department, University of Cape Town, Private Bag X3, Rondebosch 7700, South Africa*

(Received 19 June 2019; revised manuscript received 17 October 2019; published 27 December 2019)

High spin states in ^{196}Hg were populated in the ^{198}Pt$(\alpha, 6n)$ reaction at 65 MeV and γ-γ coincidence measurements were performed using the AFRODITE array at iThemba LABS. The level scheme was extended and new rotational bands were observed. A new dipole band was found. The previously reported dipole band was linked to other known states. Excitation energies, spins, and parities of all bands were determined. The bands were assigned nucleon configurations based on cranked shell model calculations.

DOI: 10.1103/PhysRevC.100.064321

I. INTRODUCTION

Mercury nuclei exhibit a number of different and interesting phenomena. The coexistence of prolate and oblate shapes has been reported for both odd- and even-mass Hg isotopes with $A \leqslant 190$ [1], and in ^{179}Hg a striking triple shape coexistence has been observed [2]. The Hg isotopes with $A \geqslant 187$ show moderately oblate deformed shapes near their ground state and at moderate spin [3–5]. At higher spins, in addition to the normal deformed shape (which might become triaxial [6,7]), the heavier Hg isotopes (with masses between 189 and 194) show rotational bands belonging to a secondary superdeformed potential-energy minimum [8,9]. The superdeformed shape in these nuclei corresponds to a ratio between the nuclear axes of approximately 1.7. In addition to the different nuclear shapes, the heavier Hg isotopes also show very interesting rotational bands, built of $M1$ and $E2$ transitions. Shears bands, produced as a result of magnetic rotation, are well known in the neighboring Pb isotopes [10]. The shears bands are generated by a gradual realignment of the angular momenta of the valence protons (initially aligned along the symmetry axis) and neutrons (initially aligned perpendicular to the symmetry axis) towards a tilted rotational axis (for a review see Ref. [11]). The dipole bands in ^{191}Hg [6], ^{192}Hg [12], ^{193}Hg [13], ^{194}Hg [14], ^{195}Hg [15], and ^{196}Hg [7], however, seem to be different. In the Pb isotopes these structures involve deformation-aligned $h_{9/2}$ and $i_{13/2}$ protons, while in Hg rotation-aligned $h_{11/2}$ protons play a major role. Such differences in the proton configurations are revealed by the low values of the $B(M1)/B(E2)$ ratios in the Hg isotopes. The structures observed at low to moderate spin in the heavier Hg isotopes result mainly from excitations of $i_{13/2}$ and low-j ν_j ($\nu_j = p_{3/2}, f_{7/2}, p_{1/2}$) neutrons. The cranked shell model had been successfully used to describe Routhians, band crossing frequencies, and alignments in these oblate nuclei [16,17].

The main features of the known level scheme of ^{196}Hg [18] are a positive-parity band up to spin 26^+ and two negative-parity sequences, one up to a 23^- and the other up to a 12^- level. Two band crossings (AB and CD) are known in the positive-parity band and one in the odd-spin negative-parity band (BC).

In this work the level scheme of ^{196}Hg was considerably extended by placing 61 new γ-ray transitions and 32 new levels in the level scheme. The additions included three new rotational bands and one new dipole band. A second dipole band was linked and spin, parity, and excitation energy were determined. Preliminary results from this study were previously reported in Ref. [19].

II. EXPERIMENT

The experiment was performed at iThemba LABS, South Africa, using the ^{198}Pt$(\alpha, 6n)^{196}$Hg reaction at 67 MeV. The target was a 0.2mg/cm^2 self-supported Pt foil enriched to 96% in ^{198}Pt. Gamma-coincidence data of two or higher fold were obtained with the AFRODITE array [20] that consisted, at the time, of seven Compton-suppressed Clover detectors

*Corresponding author: lawrie@tlabs.ac.za

†Present address: Stanford Institute for Theoretical Physics, Department of Physics, Stanford University, Stanford, CA 94305, USA; Berkeley Center for Theoretical Physics, Department of Physics, University of California Berkeley, Berkeley, CA 94720, USA; Theory Group, Physics Division, Lawrence Berkeley National Laboratory, Berkeley, CA 94720, USA.

‡Present address: Department of Physics, Faculty of Science, The M. S. University of Baroda, Vadodara 390002, India.

§Present address: Palabora Foundation, P.O. Box 1263, Phalaborwa 1390, South Africa.

¶Present address: Department of Physics, Stellenbosch University, Private Bag x1, Matieland 7602, South Africa.

configured in two geometries; (i) six detectors at 90° and one at 135°, and (ii) four detectors at 90° and three at 135°. The first geometry was chosen in order to calibrate the AFRODITE array for lifetime measurements with the recoil shadow anisotropy method [21], for which results had been published [22,23], while the second geometry was needed to obtain angular distribution data. The data were corrected for Doppler shifts using an experimental value of $\beta = 0.23\%$, before being sorted into appropriate matrices and analyzed using RADWARE [24].

The level scheme was obtained from a symmetric γ-γ matrix for all the data, containing 5×10^8 events. In comparison the level scheme of ^{196}Hg reported in Ref. [18] was obtained from a data set of 6.5×10^7 events, while the dipole band in ^{196}Hg reported in Ref. [7] was observed in a data set of 7.5×10^7(twofold and threefold) events conditioned by multiplicity. In addition to the γ rays from ^{196}Hg we observed γ rays from ^{197}Hg (25%), ^{195}Hg (4%), and ^{194}Hg (3%) arising from competing reaction channels and from isotopic impurities in the target. Spin and parity assignments were based on linear polarization anisotropy and angular distribution ratio measurements. In this work we used angular distribution ratios given by $R_{AD} = I_\gamma(135°)/I_\gamma(90°)$, where the relevant intensities were obtained from isotropically-gated background-subtracted spectra at 135° and 90° [25]. These measurements could only utilize the data obtained with geometry (ii) having four detectors at 90° and three at 135° (approximately 10^8 events). The R_{AD} values were not normalized for the difference in efficiency at each angle, but were benchmarked based on the average measured R_{AD} for known stretched quadrupole and stretched electric dipole transitions above the isomers. For dipole transitions a value of 0.50 ± 0.02 is obtained for the known 468- and 853-keV $E1$ transitions, while the average R_{AD} for quadrupoles is 0.86 ± 0.02 for transitions above the known isomers. Below the isomers R_{AD} can be affected by loss of alignment during the recoil into vacuum, as well as by the shadow effect of the clover detector collimators. The measured value for quadrupole transitions is 0.66 in this case. R_{AD} was found to be insensitive to the multipolarity of the gating transition; thus, where possible, average values for more than one gate were used.

Linear polarization measurements were performed as described in Ref. [26] and used data from geometry (i) with six detectors at 90°. Gated and background subtracted spectra for horizontal and for vertical Compton-scattered events in a clover detector were generated and the polarization anisotropy was calculated as $A_p = (A_\perp - \varepsilon A_\parallel)/(A_\perp + \varepsilon A_\parallel)$, where $A_\parallel$ and $A_\perp$ denote the areas of the peaks of interest measured in the spectra for horizontal and for vertical Compton-scattered events respectively, and ε is the efficiency for horizontal relative to vertical Compton-scattered events for unpolarized γ rays. Here $\varepsilon = 1$ was confirmed with source measurements. For pure stretched transitions the polarization anisotropy is positive for transitions with electric nature and negative for magnetic transitions. The average polarization anisotropy for nine transitions with known electric quadrupole nature was 0.098 ± 0.015 with a standard deviation of 0.01, while for the two known magnetic transitions values of -0.10 ± 0.08 and -0.09 ± 0.07 were obtained. For $E2$ transitions below the isomeric states values between 0.02 ± 0.01 and 0.04 ± 0.01 were obtained.

Gamma-ray intensities were measured using spectra gated from below the relevant transition, corrected for efficiency and appropriately normalized. The intensity of the 636-keV transition relative to the 426-keV transition had to be corrected for the contribution to the 636-keV peak from ^{194}Hg contamination. In some cases intensities of weak transitions could be more reliably determined from the branching ratio measured by gating above the level, and using the absolute intensity of the stronger branch obtained from a gate below.

III. RESULTS

The partial level schemes for ^{196}Hg obtained in the present study are given in Fig. 1 for the negative-parity and dipole bands, and in Fig. 2 for the positive-parity bands. Band labels refer to the band both below and above any band crossings. Details of level and γ-ray properties are presented in Table I.

A. Negative-parity bands

As shown in Fig. 1, the present work confirms the odd-spin negative-parity band (Band 2) as reported by Mehta *et al.* [18] up to the 23^- level at 5959 keV and an additional level at 7032 keV is added at the top of the band. The multipolarity of the new 1074-keV γ ray could not be established due to low statistics.

Coincidence relationships from the present experiment confirm the levels and transitions of the previously reported [18,27] even-spin negative-parity sequence (Band 3) up to 3237 keV, and allow an extension of the band up to a 24^- level at 6778 keV by placing the sequence of γ rays with energies of 665, 303, 343, 509, 723, and 999 keV as indicated in Fig. 1. Also observed are a number of transitions linking this band to the odd-spin negative-parity band, Band 2. The 665-keV γ ray is clearly observed in coincidence with the 683-keV transition and not with, for instance, the 690-keV transition of Band 2. The proposed 302.6-keV transition is observed in spectra gated on both the 489- and 257-keV transitions that are in anticoincidence with the 300- and 302-keV transitions of Band 4. Furthermore it shows a significant energy shift relative to the 300- and 302-keV transitions observed in spectra gated on the 571-keV transition of Band 4. Finally, this placement is confirmed by the coincidence relationships of the 229-keV transition. The 343-keV transition can be unambiguously placed above the 4205-keV level and the observed coincidence relationships of the 160- and 571-keV transitions confirm the level at 4547 keV. A 509-keV transition that is relatively free from contamination from the 511-keV peak is observed in coincidence with the 571- and 160-keV transitions. This transition is also observed in a gate on 343 keV. However, in this case the 509-keV line is broadened and the centroid is shifted to a lower energy, which indicates the presence of a 507.6-keV transition to the 15^- level. We further propose a 723-keV transition feeding the 5056-keV level, which has a distinctly lower energy than the $6^+ \rightarrow 4^+$ transition. The observation of the 741-keV

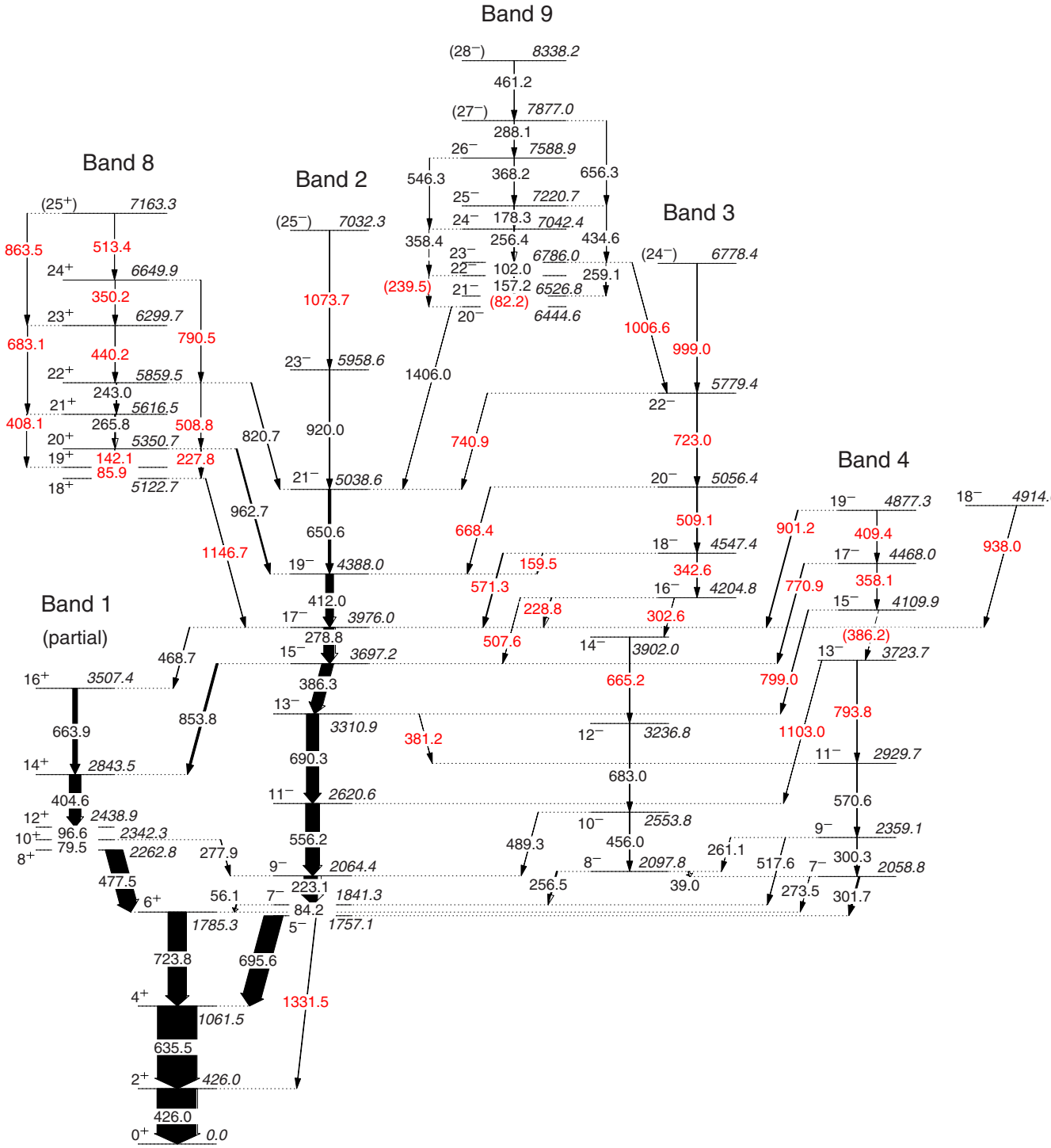

FIG. 1. A partial level scheme showing the negative-parity bands and dipole bands in ^{196}Hg. New or newly placed γ rays are shown in red.

transition to the 5039-keV level in Band 2 confirms the 5779-keV level in Band 3.

The γ-ray transitions of Band 3 are illustrated in the spectra shown in Fig. 3, and most of them can be identified in the spectrum gated on the 999- and 1007-keV transitions [see Fig. 3(a)]. Figure 3(b) illustrates the 723-keV doublet of the proposed 723.0-keV transition in Band 3 and the known 723.8-keV transition in Band 1. The peak at 723 keV, observed in the spectrum gated on the 999- and 1007-keV γ rays decaying into Band 3 (red), is shifted by 0.5 keV to a lower energy relative to the peak observed in the spectrum gated on the 920- and 1406-keV γ rays (blue), where the peak corresponds to the 723.8 keV transition from Band 1. The shift of the peak in the former gated spectrum suggests the presence of the second member of the 723-kev doublet, the 723.0 keV transition that belongs to Band 3. The spectrum gated on the 343-keV γ ray in Band 3 illustrates the transitions in the lower-spin part of Band 3 [see Fig. 3(c)].

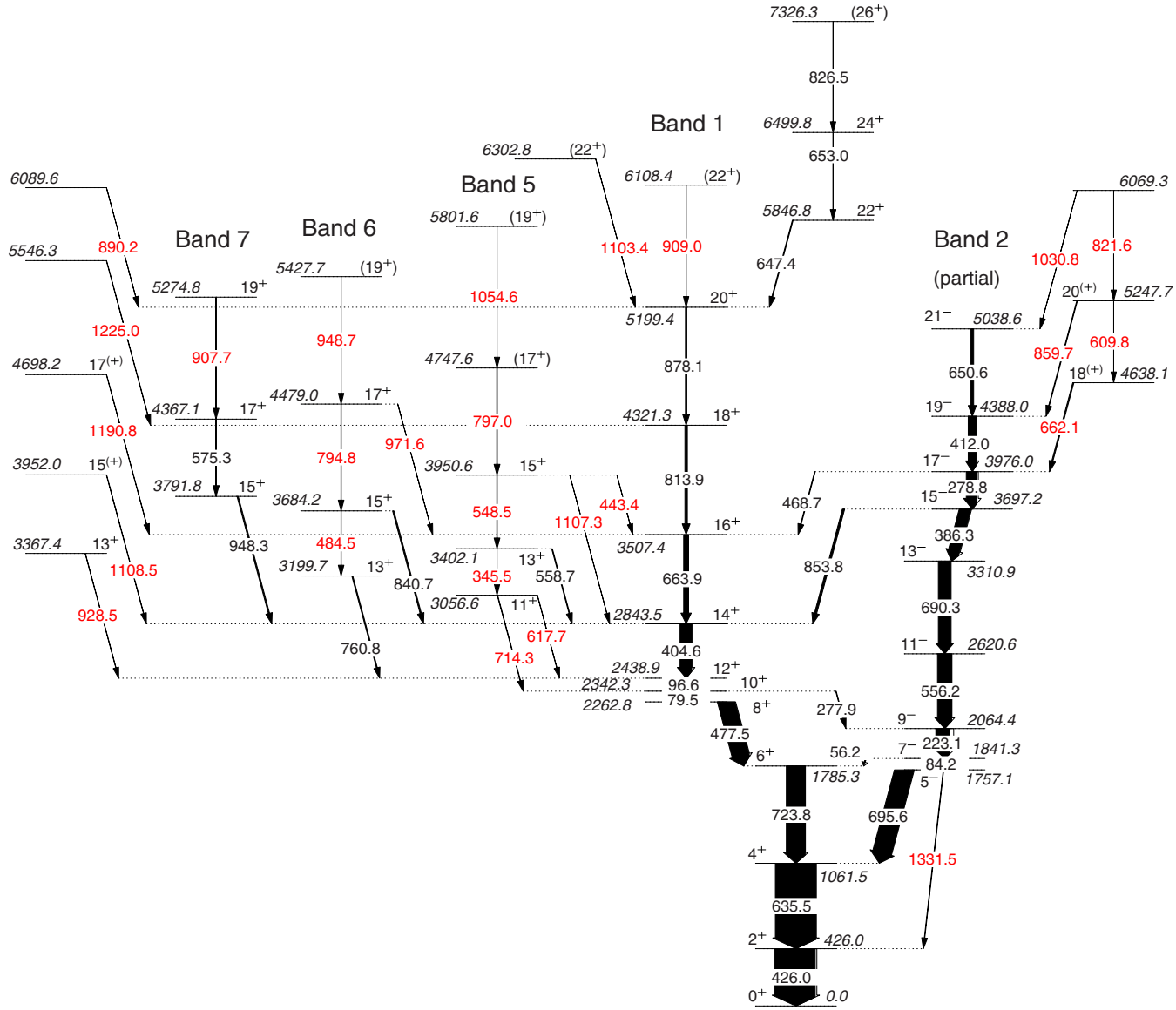

FIG. 2. A partial level scheme showing the positive-parity bands in ^{196}Hg. New or newly placed γ rays are shown in red.

The previously reported levels at 2059, 2359, and 2930 keV (placed in Band 4) and the γ-ray decays from these levels [18,27] are confirmed in the present work, but with a change of spin as shown in Fig. 1. R_{AD} and polarization asymmetry measurements suggest an assignment of a stretched $E1$ nature to the 274-keV transition between the 2059-keV level and the 6^+ level at 1785 keV. The 2059-keV level is thus assigned spin and parity of 7^- as opposed to the previous tentative assignment of 6^- [18] that was not based on angular distribution measurements. The angular distribution ratio for the 518-keV transition is consistent with that of a stretched quadrupole, in agreement with the angular distribution coefficients in Ref. [27]. Since the R_{AD} for the 300.3-keV transition obtained from a spectrum gated on the 274-keV transition indicates a stretched quadrupole nature, the 2059-keV level is placed as the bandhead of Band 4 instead of in Band 3 as previously reported [18,27]. A spin and parity assignment of 11^- for the 2930-keV level of this band is similarly made based on the R_{AD} values obtained with a gate on the 274-keV γ ray. This band is extended up to a 19^- level at 4877 keV, with spins and parities based on the measured multipole order of the relatively strong 799-, 771-, and 901-keV transitions to Band 2. In addition a 381-keV $E2$ transition is found to link Bands 2 and 4, lending further support to the spin and parity assignments of Band 4. A spectrum to illustrate the transitions of Band 4 is shown in Fig. 4.

B. Positive-parity bands

The positive-parity bands observed in the present work are shown in Fig. 2. The known ground-state band and its extension beyond the first and second band crossings [18] are confirmed up to the 26^+ level at 7326 keV (Band 1). A newly observed 909-keV transition that is not in coincidence with the 647- or 653-keV transitions is placed above the 5199-keV level.

TABLE I. Energy, intensity, Angular distribution ratio, linear polarization asymmetry, and multipolarity. The energy of the initial state as well as the spins and parities of initial and final states are also given, except where there is insufficient evidence to make firm or tentative assignments. Reduced R_{AD} values for $E2$ transitions below isomers are marked with a ‡ (see text).

E_γ (keV)	I_γ	R_{AD}	A_p	ML	E_i	$I_i^\pi \rightarrow I_f^\pi$
(39.0)					2097.8	$8^- \rightarrow 7^-$
56.1(3)					1841.3	$7^- \rightarrow 6^+$
79.5(3)	2.47(30)	0.71(5)			2342.3	$10^+ \rightarrow 8^+$
(82.2)					6526.8	$21^- \rightarrow 20^-$
84.2(2)	3.9(4)	0.82(5)			1841.3	$7^- \rightarrow 5^-$
85.9(3)	0.28(9)				5208.4	$19^+ \rightarrow 18^+$
96.6(1)	5.1(5)	0.80(3)			2438.9	$12^+ \rightarrow 10^+$
102.0(2)	0.16(2)	0.56(18)			6786.0	$23^- \rightarrow 22^-$
142.1(2)	0.36(4)	0.47(9)			5350.7	$20^+ \rightarrow 19^+$
157.2(2)	0.40(8)	0.53(7)			6684.0	$22^- \rightarrow 21^-$
159.5(3)	0.33(6)	0.79(15)			4547.4	$18^- \rightarrow 19^-$
178.3(3)	0.40(8)	0.47(7)			7220.7	$25^- \rightarrow 24^-$
223.1(1)	34.8(15)	0.84(1)	0.11(1)	$E2$	2064.4	$9^- \rightarrow 7^-$
227.8(5)	0.21(4)				5350.7	$20^+ \rightarrow 18^+$
228.8(2)	0.91(9)	0.69(5)	0.06(8)	$M1+E2$	4204.8	$16^- \rightarrow 17^-$
(239.5)					6684.0	$22^- \rightarrow 20^-$
243.0(2)	0.58(10)	0.55(5)	−0.08(6)	$M1$	5859.5	$22^+ \rightarrow 21^+$
256.4(3)	1.08(10)	0.47(5)	−0.06(7)	$M1$	7042.4	$24^- \rightarrow 23^-$
256.5(2)	2.00(20)	0.48(3)	−0.08(6)	$M1$	2097.8	$8^- \rightarrow 7^-$
259.1(5)	0.24(8)				6786.0	$23^- \rightarrow 21^-$
261.1(3)	0.20(5)				2359.1	$9^- \rightarrow 8^-$
265.8(2)	1.64(15)	0.46(3)	−0.08(6)	$M1$	5616.5	$21^+ \rightarrow 20^+$
273.5(3)	0.37(4)	0.39(10)	0.21(16)	$E1$	2058.8	$7^- \rightarrow 6^+$
277.9(2)	1.28(10)				2342.3	$10^+ \rightarrow 9^-$
278.8(1)	26.4(13)	0.87(2)	0.12(1)	$E2$	3976.0	$17^- \rightarrow 15^-$
288.1(3)	0.37(4)				7877.0	$27^- \rightarrow 26^-$
300.3(5)	0.90(20)	0.83(11)			2359.1	$9^- \rightarrow 7^-$
301.7(5)	3.6(6)	0.78(10)			2058.8	$7^- \rightarrow 5^-$
302.6(3)	0.27(6)	0.79(15)			4204.8	$16^- \rightarrow 14^-$
342.6(2)	1.11(15)	0.82(12)	0.089(8)	$E2$	4547.4	$18^- \rightarrow 16^-$
345.5(3)	0.44(6)	0.96(18)			3402.1	$13^+ \rightarrow 11^+$
350.2(3)	0.45(10)				6649.9	$24^+ \rightarrow 23^+$
358.1(3)	0.95(10)				4468.0	$17^- \rightarrow 15^-$
358.4(4)	0.28(5)				7042.4	$24^- \rightarrow 22^-$
368.2(2)	0.52(10)	0.58(15)	−0.06(5)	$M1$	7588.9	$26^- \rightarrow 25^-$
381.2(3)	0.59(10)	0.90(9)	0.13(13)	$E2$	3310.9	$13^- \rightarrow 11^-$
386.2(3)					4109.9	$15^- \rightarrow 13^-$
386.3(1)	28.2(14)	0.85(2)	0.10(1)	$E2$	3697.2	$15^- \rightarrow 13^-$
404.6(1)	28.9(14)	0.88(2)	0.10(2)	$E2$	2843.5	$14^+ \rightarrow 12^+$
408.1(5)	0.50(10)				5616.5	$21^+ \rightarrow 19^+$
409.4(5)	1.8(5)				4877.3	$19^- \rightarrow 17^-$
412.0(1)	19.4(10)	0.87(2)	0.09(1)	$E2$	4388.0	$19^- \rightarrow 17^-$
426.0 (1)	100.0	0.65(2)‡	0.03(1)	$E2$	426.0	$2^+ \rightarrow 0^+$
434.6(5)	0.54(10)				7220.7	$25^- \rightarrow 23^-$
440.2(3)	1.03(8)	0.50(10)			6299.7	$23^+ \rightarrow 22^+$
443.4(3)	0.30(6)	0.53(15)			3950.6	$15^+ \rightarrow 16^+$
456.0(1)	2.10(20)	0.82(6)	0.05(5)	$E2$	2553.8	$10^- \rightarrow 8^-$
461.2(5)	1.0(10)				8338.2	$28^- \rightarrow 27^-$
468.7(2)	1.49(15)	0.51(3)	0.08(4)	$E1$	3976.0	$17^- \rightarrow 16^+$
477.5 (1)	42.6(21)	0.68(2)‡	0.04(1)	$E2$	2262.8	$8^+ \rightarrow 6^+$
484.5(3)	0.63(12)	0.92(10)			3684.2	$15^+ \rightarrow 13^+$
489.3(2)	0.79(4)	0.54(12)	−0.10(8)	$M1$	2553.8	$10^- \rightarrow 9^-$
507.6(5)	0.35(6)				4204.8	$16^- \rightarrow 15^-$
508.8(5)	0.55(10)	0.76(15)			5859.5	$22^+ \rightarrow 20^+$

TABLE I. *(Continued.)*

E_γ (keV)	I_γ	R_{AD}	A_p	ML	E_i	$I_i^\pi \rightarrow I_f^\pi$
509.1(5)	2.5(5)	0.99(20)	0.08(5)	$E2$	5056.4	$20^- \rightarrow 18^-$
513.4(5)	0.50(8)				7163.3	$25^+ \rightarrow 24^+$
517.6(2)	1.01(10)	0.74(9)	0.06(10)	$E2$	2359.1	$9^- \rightarrow 7^-$
546.3(3)	0.14(5)				7588.9	$26^- \rightarrow 24^-$
548.5(3)	1.07(10)	0.87(11)	0.05(10)	$E2$	3950.6	$15^+ \rightarrow 13^+$
556.2(1)	35.0(15)	0.84(2)	0.10(1)	$E2$	2620.6	$11^- \rightarrow 9^-$
558.7(2)	1.6(3)				3402.1	$13^+ \rightarrow 14^+$
570.6(2)	1.9(6)	0.81(10)	0.06(3)	$E2$	2929.7	$11^- \rightarrow 9^-$
571.3(3)	2.01(20)	0.78(12)	−0.12(7)	$M1+E2$	4547.4	$18^- \rightarrow 17^-$
575.3(2)	1.99(20)	0.86(8)			4367.1	$17^+ \rightarrow 15^+$
609.8(5)	0.40(8)	0.82(12)			5247.7	$20^{(+)} \rightarrow 18^{(+)}$
617.7(5)	0.55(20)				3056.6	$11^+ \rightarrow 12^+$
635.5 (1)	100.0(20)	0.65(1)[‡]	0.02(1)	$E2$	1061.5	$4^+ \rightarrow 2^+$
647.4(3)	1.80(20)	0.86(6)	0.05(4)	$E2$	5846.8	$22^+ \rightarrow 20^+$
650.6(2)	6.6(6)	0.87(3)	0.10(3)	$E2$	5038.6	$21^- \rightarrow 19^-$
653.0(3)	0.65(10)	1.08(20)	−0.04(12)		6499.8	$24^+ \rightarrow 22^+$
656.3(5)	0.47(15)				7877.0	$27^- \rightarrow 25^-$
662.1(5)	2.8(5)	0.39(8)			4638.1	$18^{(+)} \rightarrow 17^-$
663.9(2)	12.1(6)	0.85(3)	0.08(2)	$E2$	3507.4	$16^+ \rightarrow 14^+$
665.2(2)	1.17(12)	0.95(15)	0.14(5)	$E2$	3902.0	$14^- \rightarrow 12^-$
668.4(3)	1.14(17)	0.84(10)	−0.07(5)	$M1+E2$	5056.4	$20^- \rightarrow 19^-$
683.0(2)	1.75(20)	0.83(8)	0.08(6)	$E2$	3236.8	$12^- \rightarrow 10^-$
683.1(3)	0.45(10)				6299.7	$23^+ \rightarrow 21^+$
690.3(1)	31.3(15)	0.84(2)	0.09(1)	$E2$	3310.9	$13^- \rightarrow 11^-$
695.6(1)	47.6(20)	0.51(2)	0.01(1)	$E1$	1757.1	$5^- \rightarrow 4^+$
714.3(3)	1.05(15)	0.52(8)	−0.11(16)	$M1$	3056.6	$11^+ \rightarrow 10^+$
723.0(5)	2.0(8)				5779.4	$22^- \rightarrow 20^-$
723.8 (2)	46.8(20)	0.67(1)[‡]	0.03(1)	$E2$	1785.3	$6^+ \rightarrow 4^+$
740.9(5)	0.29(5)	0.79(25)			5779.4	$22^- \rightarrow 21^-$
741.3(5)	0.35(7)	0.55(12)			3941.0	$\rightarrow 13^+$ at 3199.7 keV
760.8(2)	2.3(3)	0.44(10)	−0.04(4)	$M1$	3199.7	$13^+ \rightarrow 12^+$
770.9(2)	1.63(20)	0.91(9)			4468.0	$17^- \rightarrow 15^-$
785.7(5)	0.43(8)					$\rightarrow 13^+$ at 3199.7 keV
790.5(3)	0.93(10)	0.87(13)			6649.9	$24^+ \rightarrow 22^+$
793.8(3)	0.50(5)				3723.7	$13^- \rightarrow 11^-$
794.8(4)	0.81(20)	0.99(30)			4479.0	$17^+ \rightarrow 15^+$
797.0(5)	1.29(20)				4747.6	$(17^+) \rightarrow 15^+$
799.0(3)	1.41(20)	0.81(9)	0.09(8)	$E2$	4109.9	$15^- \rightarrow 13^-$
813.9(2)	6.1(5)	0.90(3)	0.09(3)	$E2$	4321.3	$18^+ \rightarrow 16^+$
820.7(2)	1.7(4)	0.55(5)	0.07(5)	$E1$	5859.5	$22^+ \rightarrow 21^-$
821.6(3)	<0.2				6069.3	$\rightarrow 20^+$ at 5247.7 keV
826.5(3)	<0.2				7326.3	$26^+ \rightarrow 24^+$
840.7(2)	3.1(4)	0.36(8)	−0.07(5)	$M1$	3684.2	$15^+ \rightarrow 14^+$
853.8(2)	5.5(3)	0.49(2)	0.03(2)	$E1$	3697.2	$15^- \rightarrow 14^+$
859.7(3)	1.60(20)	0.46(4)	0.04(6)		5247.7	$20^{(+)} \rightarrow 19^-$
863.5(5)	0.64(12)				7163.2	$25^+ \rightarrow 23^+$
878.1(2)	3.4(3)	0.87(3)	0.08(3)	$E2$	5199.4	$20^+ \rightarrow 18^+$
890.2(5)	0.36(7)				6089.6	$\rightarrow 20^+$
901.2(3)	1.9(3)	0.81(8)	0.09(8)	$E2$	4877.3	$19^- \rightarrow 17^-$
907.7(3)	0.71(15)	0.87(25)			5274.8	$19^+ \rightarrow 17^+$
909.0(4)	0.43(8)				6108.4	$(22^+) \rightarrow 20^+$
920.0(2)	2.05(20)	0.85(7)	0.08(5)	$E2$	5958.6	$23^- \rightarrow 21^-$
928.5(5)	0.62(10)	0.30(15)			3367.4	$13^+ \rightarrow 12^+$
938.0(3)	0.65(10)	0.32(6)	−0.10(6)	$M1$	4914.0	$18^- \rightarrow 17^-$
948.3(2)	3.0(6)	0.39(3)	−0.02(3)	$M1$	3791.8	$15^+ \rightarrow 14^+$
948.7(5)	0.23(5)				5427.7	$(19^+) \rightarrow 17^+$

TABLE I. *(Continued.)*

E_γ (keV)	I_γ	R_{AD}	A_p	ML	E_i	$I_i^\pi \rightarrow I_f^\pi$
962.7(1)	3.3(3)	0.47(2)	0.06(2)	$E1$	5350.7	$20^+ \rightarrow 19^-$
971.0(3)	0.79(15)	0.90(20)			5338.2	$\rightarrow 17^+$ at 4367.1 keV
971.6(3)	0.34(5)				4479.0	$17^+ \rightarrow 16^+$
999.0(5)	0.45(10)				6778.4	$(24^-) \rightarrow 22^-$
1006.6(3)	0.53(10)	0.67(12)	0.04(9)		6786.0	$23^- \rightarrow 22^{(+)}$
1030.8(5)	0.15(5)				6069.3	$\rightarrow 22^{(+)}$
1054.6(5)	0.28(8)				5802.2	$(19^+) \rightarrow (17^+)$
1073.7(5)	0.22(4)				7032.3	$(25^-) \rightarrow 23^-$
1103.0(5)	0.20(5)				3723.7	$13^- \rightarrow 11^-$
1103.4(5)	0.42(8)	0.80(20)	0.08(14)		6302.8	$(22^+) \rightarrow 20^+$
1107.3(5)	0.27(5)				3950.6	$15^+ \rightarrow 14^+$
1108.5(5)	0.71(14)	0.50(7)			3952.0	$15^{(+)} \rightarrow 14^+$
1146.7(2)	1.24(15)	0.47(5)	0.08(5)	$E1$	5122.7	$18^+ \rightarrow 17^-$
1190.8(5)	0.54(10)	0.42(6)			4698.2	$17^{(+)} \rightarrow 16^+$
1225.0(5)	0.65(13)	0.78(11)			5546.3	$\rightarrow 18^+$
1331.5 (5)	1.17(10)	0.65(11)			1757.1	$5^- \rightarrow 2^+$
1406.0(3)	0.47(8)	0.59(12)			6444.6	$20^- \rightarrow 21^-$

The structure reported by Mehta *et al.* [18] around the 3792-keV level (Band 7) is confirmed, as is the proposed spin. We assigned positive parity to this level, and extended the structure with the placement of a 908-keV transition. In addition two new positive-parity bands, Bands 5 and 6, were identified, as shown in Fig. 2. Band 6, consisting of the 3200-, 3684-, and 4479-keV levels, is well established by the new 761-, 841-, 972-, 485-, and 795-keV transitions and their coincidence relationships. These transitions are all in coincidence with a new 948.7-keV γ ray which was placed at the top of Band 6. Transitions of Bands 6 and 7 are illustrated in Fig. 5(a). R_{AD}, and polarization asymmetries for the 761- and 841-keV transitions indicate mixed $M1 + E2$ nature while the in-band 485- and 795-keV transitions are stretched quadrupoles, thus odd spin and positive parity are assigned to Band 6.

The level structure of the new Band 5 is well established by the observed coincidence relationships between the in- and out-of-band transitions [see Figs. 5(b) and 5(c)]. Both the 714- and 443-keV transitions are shown to be stretched dipoles while the polarization asymmetry for the 714-keV γ ray indicates a magnetic nature. Furthermore both the 3057- and 3951-keV levels decay to $I_i + 1$ and $I_i - 1$ levels, leading to unambiguous spin and parity assignments for Band 5.

In Fig. 2 the new 929-, 1109-, 1191-, 1225-, and 890-keV transitions decaying to Band 1 are tentatively grouped together and might constitute an additional band; however, in-band transitions could not be observed at a sufficient

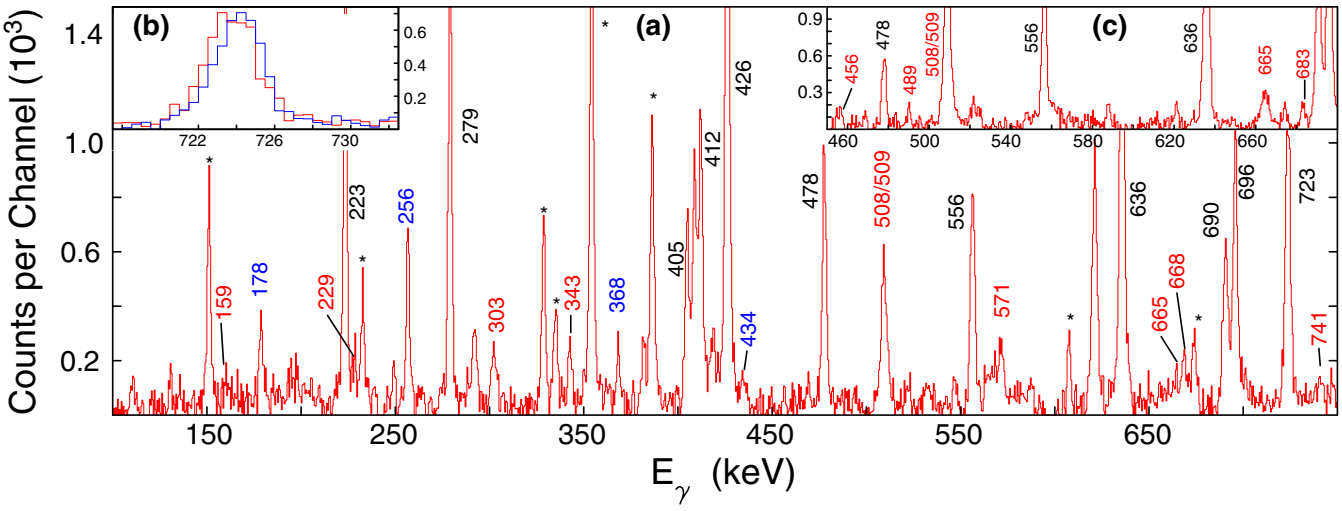

FIG. 3. Coincidence spectra to illustrate transitions in Band 3: (a) a spectrum gated on 999 and 1007 keV, (b) the region around 723 keV in spectra gated on 999 and 1006 keV (red) and on 920 and 1406 keV (blue), and (c) a spectrum gated on 343 keV. Peaks marked in red are in Band 3, peaks marked in blue are in the dipole band Band 9, while those marked with an $*$ belong to other Hg isotopes.

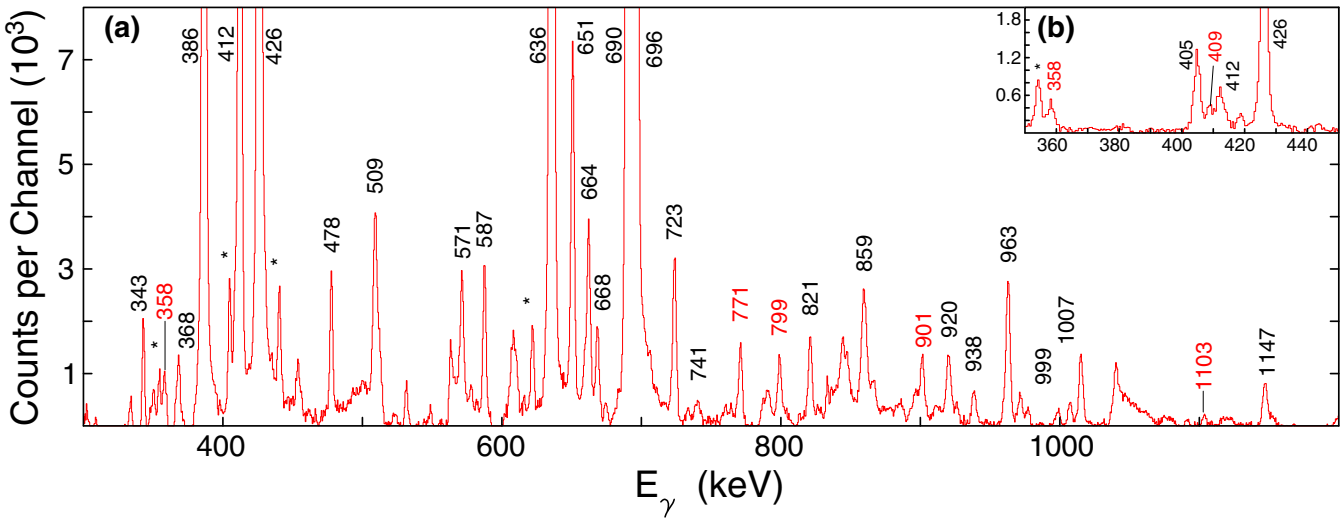

FIG. 4. Coincidence spectra to illustrate transitions in Band 4: (a) a spectrum gated on 557 keV showing the new transitions linking Bands 4 and 2; (b) a region of a spectrum gated on 799 keV illustrating the new 358- and 409-keV transitions. Peaks marked in red are in Band 3, while those marked with an ∗ belong to other Hg isotopes.

confidence level to allow inclusion in the level scheme. A structure consisting of three levels at 4638, 5248, and 6069 keV that decays to the higher energy part of Band 2 is observed, as shown in Fig. 2. The R_{AD} value for the in-band 610-keV transition is consistent with that of a stretched quadrupole, while the values for the 662- and 860-keV decays

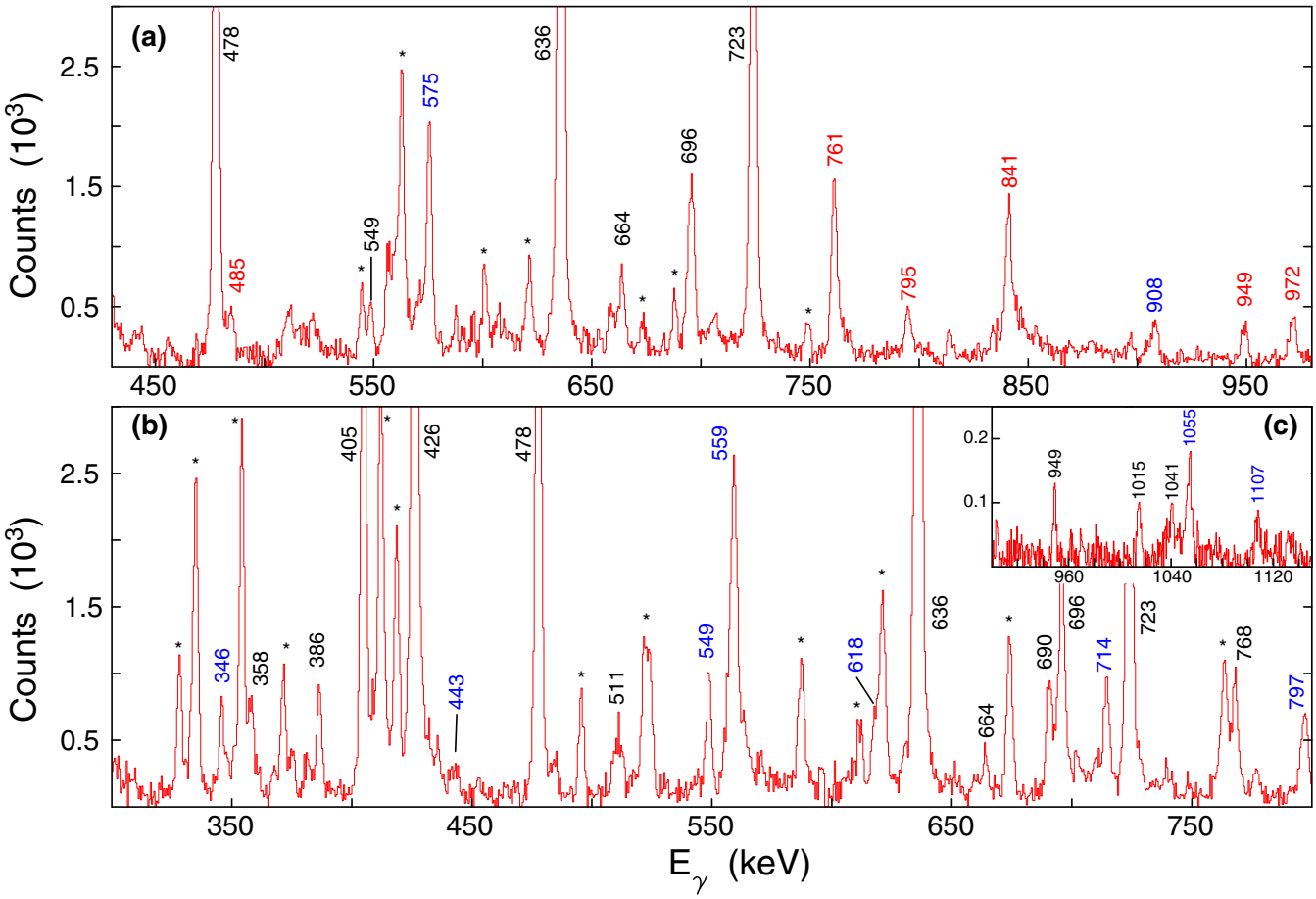

FIG. 5. Coincidence spectra showing transitions of the positive-parity bands: (a) a spectrum gated on 485, 795, and 949 keV showing transitions of Bands 6 (labeled in red) and Band 7 (labeled in blue); (b) a spectrum gated on 346, 549, and 797 keV showing transitions of Band 5 (labeled in blue); (c) an expanded region of the spectrum gated on 797 keV showing the 1055- and 1107-keV transitions of Band 5.

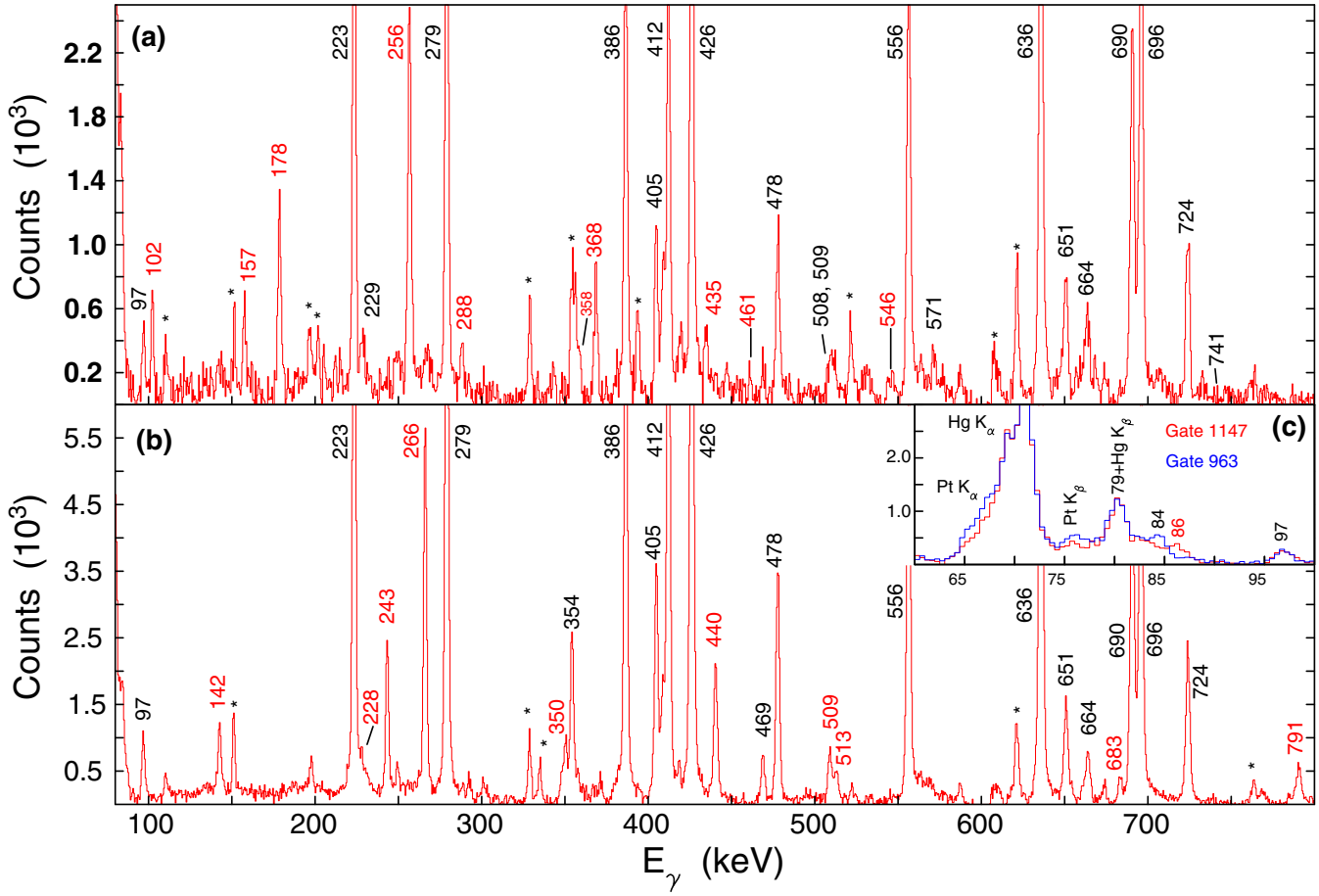

FIG. 6. Coincidence spectra showing transitions of the two dipole bands: (a) a spectrum gated on 102, 142, 368, and 288 keV showing transitions of Band 9 (red); (b) a spectrum gated on 821, 963, and 1147 keV showing transitions of Band 8 (red); (c) spectra gated on 963 keV (blue) and 1147 keV (red) respectively showing the x-ray region and illustrating the 86-keV transition in Band 8. A relative normalization was applied, based on the Hg $K\alpha$ x-ray intensity. Peaks marked with an $*$ belong to other Hg isotopes.

to Band 2 indicate stretched dipole nature. However, polarization measurements were not possible, thus a definite parity assignment could not be made.

C. Dipole bands

In the present work we observe the dipole band reported by Cederwall *et al.* [7] up to the 461-keV transition, and our R_{AD} values confirm the stretched dipole nature of the 157-, 102-, 178-, and 368-keV transitions. However, we could not positively identify the reported 398-keV $M1$ and the 859- and 749-keV $E2$ transitions. The present work allowed this band to be linked to both the odd- and even-spin negative-parity bands (Bands 2 and 3) via 1406- and 1007-keV transitions, respectively (see Fig. 1). These transitions were previously observed and were associated with the decay out of the dipole band, but were not placed, thus the band remained unconnected to the rest of the level scheme and its spin and parity assignments were tentative. The 1007-keV transition feeds into the 22^- level at 5779 keV. Furthermore the 1007-keV transition is observed in coincidence with the 256-, 178-, and 368-keV transitions but not with the 157- and 102-keV transitions [see Fig. 3(a)], thus we place the 1007-keV transition between a 6786-keV level of Band 9 (below the 256-keV transition), and the 5779-keV level as in Fig. 1. In Fig. 6(a) a spectrum from the sum of gates on 102-, 178-, 368-, and 288-keV γ rays is shown, in which most of the dipole transitions and some of the quadrupole transitions can be identified. Since R_{AD} for the 1007-keV transition is between that of a pure stretched dipole and stretched quadrupole, we propose a mixed $M1+E2$ nature for it. Thus we assign a spin and parity of 23^- for the 6786-keV level. The 1406-keV transition is in coincidence with all the transitions of the dipole band and feeds into the 5039-keV level in Band 2, as also observed in [7]. We thus propose that the 1406-keV transition depopulates a 6445-keV level that is fed from the dipole band via an unobserved 82.2-keV transition and suggest that this level may be the bandhead of Band 9. The measured R_{AD} for the 1406-keV γ ray is consistent with a stretched dipole transition, probably with mixed $M1+E2$ multipolarity. The band would thus have negative parity and a bandhead spin of 20.

Mehta *et al.* [18] reported a structure consisting of 5351-, 5617-, and 5860-keV levels, with in-band dipole transitions of 266 and 243 keV, that decay to the negative-parity band (Band 2) via 963- and 821-keV transitions. This band (Band 8) is confirmed and expanded with the addition of 3 levels

above the 5860-keV level. In addition we observed transitions of 142 and 86 keV as well as a 228-keV crossover transition that are placed below the 5351-keV level, and a 1147-keV $E2$ transition linking this band to the 17^- state in the negative-parity band. A summed spectrum gated on the 821-, 963-, and 1147-keV transitions is shown in Fig. 6(b). It illustrates the transitions of this positive-parity dipole band. Figure 6(c) shows two expanded spectra where the 86-keV γ ray placed at the bottom of Band 8 is clearly observable in the 1147-keV gate, shown in red, but is absent in the gate on 963 keV, shown in blue. R_{AD} and A_p measurements confirm that the 821-, 963-, and 1147-keV linking transitions are stretched electric dipoles, thus fixing the spin and parity of the band, while the 142-, 265-, 243-, 440-keV in-band transitions are stretched dipoles.

IV. DISCUSSION

The known level schemes of the Hg isotopes in the 190 mass region exhibit very similar features. Level energies of the yrast bands in the even-mass Hg isotopes are nearly identical up to spin 6 and show a smooth dependence on mass at higher spin for $A < 200$ [28]. This has been attributed to the fact that the structure is mostly dependent on $i_{13/2}$ neutrons outside of a weakly deformed core. The structure had been shown to be well described by the cranked shell model (CSM),which describes a rotating nucleus with stable deformation and with pairing interactions, thus combining the description of rotational bands and particle excitations in the same formalism [29]. The model calculates Routhians (the single-particle energies in a coordinate system rotating together with the nucleus) as a function of the rotational frequency and predicts several properties of the rotational bands, such as alignment, band crossing frequency, etc. The model had been used to interpret structures in ^{196}Hg in Ref. [18].

In the discussion we compare the new structures obtained in the present work to those in the neighboring Hg isotopes and to CSM calculations. As the Routhians in the CSM have only parity ($\pi = \pm$) and signature ($\alpha = \pm 1/2$) as good quantum numbers, it is customary to label them with letters. For instance the lowest-energy neutron Routhian with positive parity and positive signature, $(\pi, \alpha) = (+, +1/2)$ is labeled A, while the second lowest-energy $(+, +1/2)$ Routhian is labeled C. The lowest-energy neutron Routhian with positive parity and negative signature is labeled B, while the one with the second lowest energy is labeled D. In the case of ^{196}Hg, the four positive-parity neutron Routhians, A, B, C, and D originate from Nillson orbitals from the $i_{13/2}$ shell. The negative-parity neutron Routhians are customarily labeled as E, F, G, and H and in this case originate from low-j orbitals from the $p_{3/2}$, $f_{5/2}$, and $p_{1/2}$ shells. The proton Routhians are usually labeled with lower-case letters. For more details on the CSM labels see Table II.

Cranked shell model calculations [29] were performed with a Nilsson potential that used the l-dependent parameter set from Hübel *et al.* [17] and deformation parameters of $\varepsilon_2 = 0.117$, $\varepsilon_4 = -0.03$, $\gamma = -62.4^\circ$ which were obtained from total Routhian surface calculations [30] at $\hbar\omega = 0.1$ MeV (see Fig. 7). The CSM calculations were carried out with neutron and proton pairing energies fixed at 1.0 and 0.5 MeV respectively as in Ref. [17]. The Fermi surface was set at 41.0 MeV for protons and 51.6 MeV for neutrons. Neutron and proton quasiparticle Routhians are shown in Fig. 8, and the calculated properties, summarized in Table II, are in reasonable agreement with the calculated values in Ref. [17,18].

TABLE II. Properties of single-particle Routhians in ^{196}Hg.

Routhian	Parity and signature	Alignment	Shell model state
neutrons			
A	$(+, +1/2)$	6.47	$i_{13/2}$
B	$(+, -1/2)$	5.38	
C	$(+, +1/2)$	4.26	$i_{13/2}$
D	$(+, -1/2)$	3.16	
E	$(-, +1/2)$	2.27	$p_{3/2}/f_{5/2}/p_{1/2}$
F	$(-, -1/2)$	1.54	
G	$(-, +1/2)$	0.46	$p_{3/2}/f_{5/2}/p_{1/2}$
H	$(-, -1/2)$	1.33	
protons			
a	$(+, +1/2)$	0.34	$s_{1/2}/d_{3/2}$
b	$(+, -1/2)$	0.54	
e	$(-, +1/2)$	0.84	$h_{9/2}$
f	$(-, -1/2)$	0.84	
g	$(-, +1/2)$	4.31	$h_{11/2}$
h	$(-, -1/2)$	5.47	

For a comparison between the calculations and experimental values the data were converted to the rotational frame using Harris parameters of $J_0 = 8\ \hbar^2/\text{MeV}$ and $J_1 = 40\ \hbar^4/\text{MeV}^3$ that are appropriate to this mass region [17]. The experimental Routhians and aligned angular momenta for all the rotational

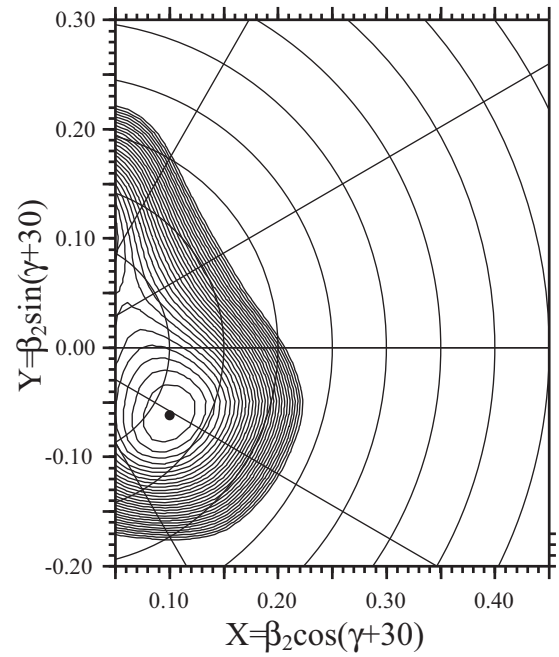

FIG. 7. Total Routhian surface calculations at a rotational frequency of $0.1\hbar\omega$.

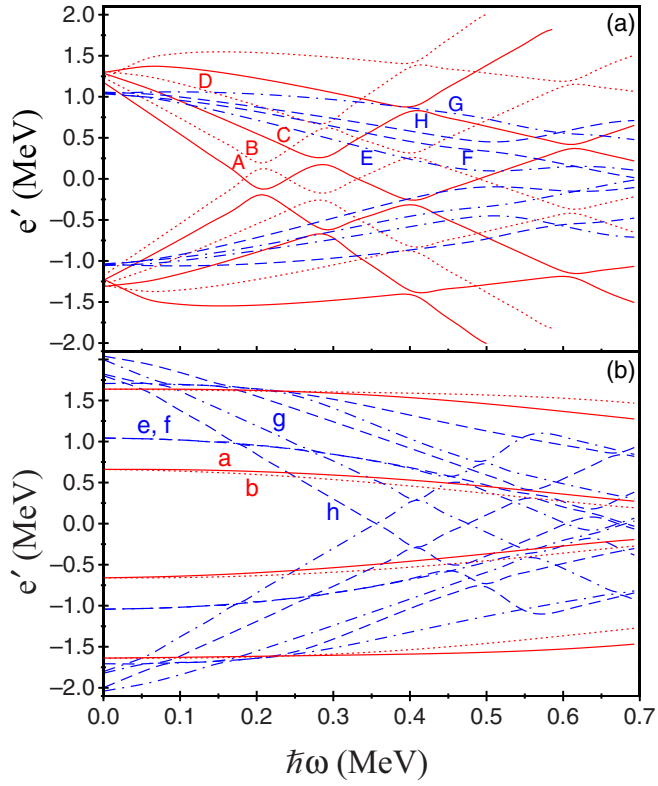

FIG. 8. Quasiparticle Routhians for neutrons (a) and protons (b). Parity and signature of states are indicated as follows: solid lines $(+, +1/2)$, dashed lines $(+, -1/2)$, dot-dashed lines $(-, +1/2)$, and dashed lines $(-, -1/2)$.

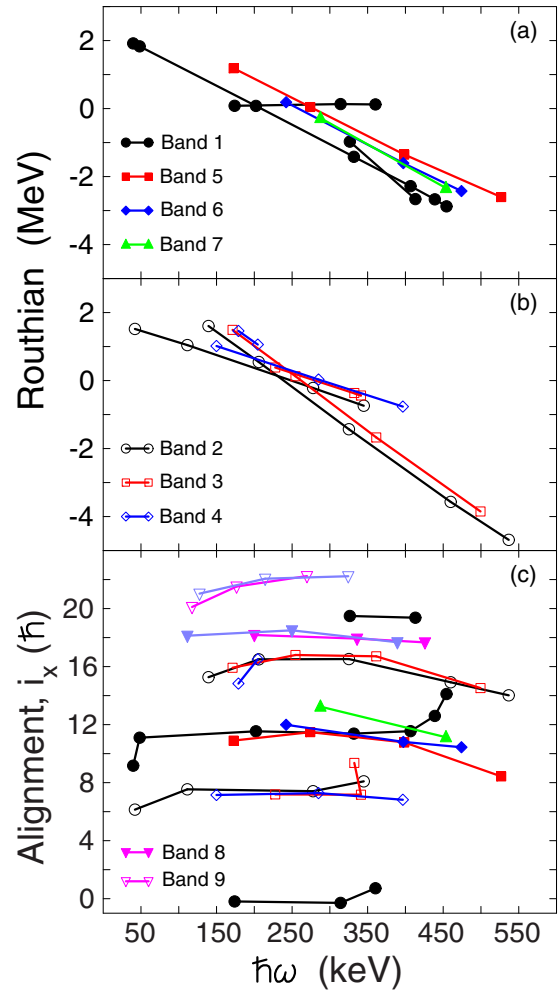

FIG. 9. Experimental Routhians and aligned angular momenta for ^{196}Hg. Harris parameters of $J_0 = 8\ \hbar^2/\text{MeV}$ and $J_1 = 40\ \hbar^2/\text{MeV}^3$ were used.

bands observed in this study are shown in Fig. 9 and the alignments and band crossing frequencies are given in Table III, together with the calculated values.

A. Negative-parity bands

Band 2 has been well established in previous work [18,27], and has been associated with AE and ABCE configurations at low and higher spins, respectively, involving $i_{13/2}$ and ν_j (where $\nu_j = p_{3/2}, f_{5/2}, p_{1/2}$) neutron orbitals (see Table II). Band 3 was also previously observed and was associated with an AF configuration. In this work it was extended beyond the band crossing and, as seen in Fig. 8, has properties very similar to those of Band 2. Thus, as for Band 2, the band crossing can be attributed to a BC alignment. The observed gain in alignment in the AF $\rightarrow$ ABCF case is almost the same as in the AE $\rightarrow$ ABCE case, but for the former the band crossing frequency is moved to a slightly higher value (see Table III). The AF alignment does not show the reduction of about $0.7\hbar$ relative to the AE configuration, as expected from the CSM calculation. The same behavior was observed in ^{192}Hg and ^{194}Hg [17]. However, the experimental alignment gain at the band crossings for both Bands 2 and 3 corresponds well with the CSM calculations.

In this work Band 4, built above the 2059-keV level, was assigned odd spin. We note that among the neighboring Hg isotopes a third negative-parity band with odd signature has only been reported in ^{192}Hg [12], where it is not observed below the BC band crossing but extends above a 17^- level. This band was assigned a four-quasiparticle $\nu i_{13/2}^3 p_{3/2}$ configuration. It decays predominantly to the yrast odd-signature negative-parity band, as is the case for Band 4 in the present work. We propose AG and ABCG configurations for Band 4 at low and higher spins, respectively. The calculated alignment and alignment gain is in good agreement with the experimental values (see Table III). In our calculations the H configuration is energetically favoured over G but we do not observe an additional even-signature negative-parity band that could be associated with AH and ABCH configurations.

In general the agreement between the experimental data and the CSM calculations is good, particularly for the alignments of the AF, AG, ABCF, and ABCG bands; see Table III. As all three bands assigned with AE, AF, AG configurations undergo a BC alignment, the band crossing frequency suggested by the model is the same. The experimental data suggest slightly lower band crossing frequencies. To improve the agreement with the model one could in principle introduce configuration-dependent pairing, as was done in Ref. [6].

TABLE III. Experimental and calculated alignments.

	Initial alignment ($\hbar$)		Final alignment ($\hbar$)		Alignment gain ($\hbar$)		Crossing frequency (keV)	
Configuration	Expt.	Theory	Expt.	Theory	Expt.	Theory	Expt.	Theory
g.s. → AB			11.5	11.8	11.5	11.8	203	205
AB → ABCD	11.5	11.8	19.4	19.3	7.9	7.5	375	405
g.s. → AE			7.4	8.7	7.4	8.7		
AE → ABCE	7.4	8.7	16.5	18.4	9.1	9.7	230	285
g.s. → AF			7.2	8.0	7.2	8.0		
AF → ABCF	7.2	8.0	16.7	17.7	9.5	9.7	247	285
g.s. → AG			7.2	6.9	7.2	6.9		
AG → ABCG	7.2	6.9	16.5	16.6	9.3	9.7	270	285
g.s. → AC			11.4	10.7	11.4	10.7		
g.s. → BD			11.4	8.5	11.4	8.5		
AB → ABEG	11.5	11.8	13.2	14.6	1.7	2.8		
ABCE → ABCE*b(e,f)*	16.5	18.4	18.2	19.5	1.7	1.4		
ABCE → ABCE*fh*	16.5	18.4	22.2	24.5	5.7	6.1		
ABCF → ABCF*fh*	16.7	17.6	22.2	23.8	5.5	6.2		

B. Positive-parity bands

In addition to the known ground-state band (Band 1 in this work) and its extension past the first and second band crossings, we identified three positive-parity bands, all with odd signature (Bands 5, 6, and 7). All three bands decay to Band 1 only and are very similar in terms of alignment (see Fig. 9). In the lighter mass Hg isotopes there are no reported bands that are similar to Bands 5, 6, and 7. The positive-parity structures designated as T in both ^{192}Hg and ^{194}Hg [17] have rather irregular energy spacings and are therefore not considered to be similar to any of the bands in ^{196}Hg. The band in ^{194}Hg above the 14^+ level at 4015 keV [17] (ABEF) is distinctly different from Bands 5, 6, and 7 in that it has only one decay to band AB but also decays to a number of levels from the negative-parity bands. Furthermore the experimental alignment of about 14.5$\hbar$ for the ABEF band in ^{194}Hg is significantly higher than that of Bands 5, 6, and 7 in the present work.

Bands 5 and 6 in the present work have alignments that are almost identical to that of Band 1 after the first band crossing (AB configuration), and thus we propose two-quasiparticle configurations of AC and BD for these bands as the only two-quasiparticle configurations that are in agreement with the observed alignment. In fact, the calculated alignment for the AC configuration of 10.7$\hbar$ is in good agreement with the experimental value of 11.4$\hbar$. The value for BD of 8.4$\hbar$ is somewhat smaller. However, should the configuration of Band 6 involve four quasiparticles, e.g., ABEG (to account for the multiple decays to the AB band), the gain in alignment for AB → ABEG would be 2.7$\hbar$, while Band 6 has the same alignment as the AB configuration in Band 1. Furthermore the energy differences between Band 1 (AB configuration) and Bands 5 and 6 are less than 700 keV, thus they are insufficient to break an additional neutron pair to form a four-quasiparticle configuration. Thus the two-quasiparticle configurations of AC and BD seem to be favored for Band 5 and 6.

Band 7, which at present consists of only three levels, could in principle be a four-quasineutron band of ABEG configuration. The calculated alignment gain with respect to the AB configuration of 2.7$\hbar$ is somewhat higher than the experimental value of 1.7$\hbar$, thus an unambiguous configuration assignment for this band could not be made.

The agreement between the experimental data and the CSM calculations for the positive-parity bands is good, particularly for the alignments of the AB and ABCD bands; see Table III. The model also reproduces the band crossing frequency for the AB alignment well, but overestimates it for the CD alignment. A better agreement with experimental data could probably be obtained by using configuration-dependent pairing [6].

C. Dipole bands

In this work we report on two bands of strong dipole transitions with weak $E2$ crossovers. Band 8 is new, except for three previously known levels at 5351, 5617, and 5860 keV [18]. The levels had tentative spin and no parity assignment. Band 9 had been observed before [7] but was not connected to the rest of the level scheme and therefore had uncertain spin, parity, and excitation energy. We assigned unambiguous spin and party to both bands as described in Sec. III.

Band 8 extends above a 18^+ level at 5123 keV and decays via three γ-ray transitions to levels above the band crossing of the negative-parity Band 2 (ABCE). It is estimated that the 1147-keV transition corresponds to about 50% of the intensity of the band below the 5351-keV level, thus additional unobserved decay paths are likely. Band 9 has negative parity and a bandhead at spin 20. Two decays, to Bands 2 and 3 respectively, are observed but these transitions correspond to less than 40% of the intensity of the band, thus additional unobserved decay paths are again likely.

Both bands exhibit regular energy spacing, no staggering, and $B(M1)/B(E2)$ ratios of less than 3 $\mu_N^2/(e\mathrm{b})^2$ (see Fig. 10). They are thus different from the shears bands in the Pb

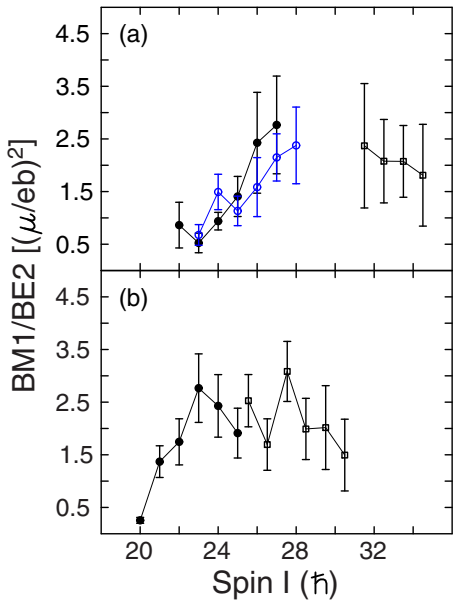

FIG. 10. Experimental $B(M1)/BE(2)$ ratios for (a) negative-parity and (b) positive-parity dipoles bands in ^{195}Hg and ^{196}Hg. Filled circles are from the present work, open circles are for ^{196}Hg from [7] shifted by $-1\hbar$, and open squares are for the dipole bands in ^{195}Hg [15].

neighbors, which are characterized by a sharp decrease in the $B(M1)$ values. This sharp decrease is caused by the nature of the shears bands. These bands are built on single-particle configurations associated with large angular momenta along the symmetry axis (proton angular momentum) and perpendicular to the symmetry axis (neutron angular momentum). The increase in the angular momentum along the band is caused by the realignment of the proton and neutron angular momenta away from the major nuclear axis and along a tilted axis. This realignment causes the perpendicular (to the tilted axis) component of the single-particle angular momenta to decrease, causing the sharp drop in the $B(M1)$ values which is characteristic for shears bands. For more details on the shears mechanism see Ref. [11]. The $B(M1)/B(E2)$ ratios for Bands 8 and 9, shown in Fig. 10, are compared with those of the dipole bands in ^{195}Hg [15] and with the values for the dipole band of ^{196}Hg [7]. For comparison the latter was shifted down by $1\hbar$ to accommodate the different spin assignment in the present work. The measured $B(M1)/B(E2)$ values for Band 9 from the present work agree, within error bars, with the previous values [7].

Dipole bands with similarly small $B(M1)/B(E2)$ ratios have been reported in all the $A = 191$–195 Hg isotopes. The band in ^{191}Hg [6] has irregular energy spacing and was not considered to have a collective nature. In ^{192}Hg the dipole band designated as Band (b) [12], also has irregular energy spacing and decays only to positive-parity structures. However, the negative-parity band in ^{192}Hg, Band (a), could be compared to Band 9 in this work, particularly since it also decays to both ABCE and ABCF bands. Of the three dipole bands in ^{193}Hg the positive-parity Structure 3 [13] had previously been considered to be non-collective [31]. The the negative-parity Structures 1 and 2 decay through a complex set of levels that are assumed to be of a single-particle nature, in contrast to the direct decay to rotational bands observed in ^{191}Hg. Structure 2 in ^{194}Hg [14] could be considered as similar to Band 8 in ^{196}Hg, if it can be assumed that this structure has positive parity. The bands that look most similar to the dipole bands in ^{196}Hg are in ^{195}Hg [15], where two bands, with positive and negative parity respectively, are observed. The decays out of these bands feed the lowest-energy negative-parity band, as in ^{196}Hg, although the positive-parity Structure 2 also feeds into the positive-parity yrast band. Except for the case of ^{195}Hg the dipole bands in the other Hg isotopes exhibit very fragmented decay via structures of irregularly spaced levels that are not observed in this work.

In assigning a configuration to Band 8 of ^{196}Hg it should be noted that all three of the observed decays go to the upper region of Band 2, which has a four-quasiparticle $\nu i^3_{13/2}\nu_j$ configuration (ABCE). This suggests that the dipole band could involve the same neutron configuration which is coupled to a two-proton excitation. The energy difference of approximately 1 MeV between the bandheads of this dipole band and the ABCE band allows for the breaking of a proton pair. Thus a six-quasiparticle $\pi h_{9/2}d_{3/2}/s_{1/2} \otimes \nu i^3_{13/2}\nu_j$ configuration is proposed for Band 8. It is the lowest-energy six-quasiparticle configuration with positive parity, and corresponds to the ABCE*be* or ABCE*bf* configuration in terms of the CSM. The *b* Routhian has a slightly higher alignment gain of $1.43\hbar$ than the *a* Routhian, while the *e* and *f* Routhians are degenerate up to high rotational frequency and have negligible alignment as they correspond to deformation aligned $h_{9/2}$ orbitals. The calculated gain in alignment of the ABCE*be* and ABCE*bf* configurations of $1.4\hbar$ with respect to the ABCE configuration is in reasonable agreement with the experimental alignment gain of $1.7\hbar$. The alignments of the two signature sequences ABCE*be* and ABCE*bf* are identical, in agreement with the experimental observations (see Fig. 9).

Band 9 decays to Bands 2 and 3 with ABCE and ABCF configurations. Thus we can assume that this dipole band involves these four-quasiparticle neutron configurations. The experimentally observed alignment gain of $5.7\hbar$ of the dipole band with respect to the ABCE and ABCF bands can be explained by involving an $h_{11/2}$ and an $h_{9/2}$ proton that are aligned along the rotation and symmetry axes respectively. The CSM calculations yield alignment gains of $6.3\hbar$ and $5.2\hbar$ for the coupling of *e* or *f* Routhians to the *h* Routhian and to the *g* Routhian, respectively. However, since the *h* Routhian is lower in energy we propose fh as the preferred proton configuration. It can be noted that both decays out of the dipole band change signature (odd signature decays to even signature and vice versa), thus the proton configuration is likely to be fh for both signature sequences in the dipole band, corresponding to the ABCE$fh \rightarrow$ ABCE and ABCF$fh \rightarrow$ ABCF decays. Thus we assign the ABCEfh and ABCFfh configurations to Band 9. The assigned configurations do not involve high-K protons, which would have been mandatory for bands with a shears nature. The assignments are in agreement with our previous considerations that the low values of the $B(M1)/B(E2)$ ratios and their smooth trend as a function of spin do not imply a shears nature for the bands in ^{196}Hg. This conclusion supports

the previous suggestion of Cederwall *et al.* [7] that Band 9 probably has a single-particle structure different from that of a shears band.

V. SUMMARY

In the present γ-spectroscopy study the known level scheme of ^{196}Hg has been considerably extended. The second negative-parity band was extended with the addition of six new levels that include a band crossing. A third negative-parity band was established by adding four new levels to the top of the band, again including a band crossing, and by changing the spin of the band. The higher-energy negative-parity bands are connected to the yrast negative-parity band by a number of new and relatively strong transitions. Two new positive-parity bands were observed, both extending up to spin 19. An additional level was added above the two known positive-parity bands. All three positive-parity bands decay to the yrast band only. The previously known dipole band observed by Cederwall *et al.* [7] was connected to two negative-parity bands, and its spin and parity were determined. A new dipole band was firmly established based on the three previously observed levels [18] through the addition of five new $M1$ transitions as well as six $E2$ crossover transitions. The $B(M1)/B(E2)$ ratios for both dipole bands are less than 3 $\mu_N^2/(e\mathrm{b})^2$ and the $E2$ energies show a regular increase associated with rotational structures. All rotational bands were interpreted in the CSM framework. Apart from the dipole bands all the positive- and negative-parity bands could be interpreted using neutron configurations only. The negative-parity bands are interpreted as $\nu i_{13/2}\ \nu_j$ and $\nu i_{13/2}^3\ \nu_j$ configurations at low and higher spins respectively, while the two new positive-parity bands are likely to have $\nu i_{13/2}^2$ configurations. The third positive-parity band might have a four-quasiparticle nature. We suggest that both dipole bands involve proton excitations and propose six-quasiparticle configurations of ABCE*b(e,f)* and ABC(E,F)*fh* configurations for the positive- and negative-parity dipole bands, respectively.

ACKNOWLEDGMENTS

We are thankful to the accelerator staff of iThemba LABS for beam delivery and to the National Research Foundation for financial support.

[1] L. P. Gaffney, M. Hackstein, R. D. Page, T. Grahn, M. Scheck, P. A. Butler, P. F. Bertone, N. Bree, R. J. Carroll *et al.*, Phys. Rev. C **89**, 024307 (2014).
[2] D. G. Jenkins, A. N. Andreyev, R. D. Page, M. P. Carpenter, R. V. F. Janssens, C. J. Lister, F. G. Kondev, T. Enqvist, P. T. Greenlees *et al.*, Phys. Rev. C **66**, 011301(R) (2002).
[3] J. Bonn, G. Huber, H.-J. Kluge, and E. W. Otten, Z. Phys. A **276**, 203 (1976).
[4] A. Bockisch, K. Bharuth-Ram, A. M. Kleinfield, and K. P. Lieb, Z. Phys. A **291**, 245 (1979).
[5] P. Dabkiewicz, F. Buchinger, H Fischer, H.-J. Kluge, H Kremmling, T. Kühl, A. C. Müller, and H. A. Schuessler, Phys. Lett. B **82**, 199 (1979).
[6] D. Ye *et al.*, Nucl. Phys. A **537**, 207 (1992).
[7] B. Cederwall, M.-A. Deleplanque, F. Azaiez, R. M. Diamond, P. Fallon, W. Korten, I.-Y. Lee, A. O. Macchiavelli, J. R. B. Oliveira *et al.*, Phys. Rev. C **47**, R2443 (1993).
[8] B. Singh, R. B. Firestone, and S. Y. S. Chu, Nucl. Data Sheets **78**, 1 (1996).
[9] X.-L. Han and C.-L. Wu, At. Data Nucl. Data Tables **63**, 117 (1996).
[10] A. K. J. Amita and B. Singh, At. Data Nucl. Data Tables **74**, 283 (2000).
[11] R. M. Clark and A. O. Macchiavelli, Annu. Rev. Nucl. Part. Sci **50**, 1 (2000).
[12] Y. Le Coz *et al.*, Z. Phys. A **348**, 87 (1994).
[13] N. Fotiades *et al.*, J. Phys. G: Nucl. Part. Phys. **21**, 911 (1995).
[14] N. Fotiades *et al.*, Z. Phys. A **354**, 169 (1996).
[15] N. Nenoff *et al.*, Nucl. Phys. A **629**, 621 (1998).
[16] M. Guttormsen and H. Hübel, Nucl. Phys. A **380**, 502 (1982).
[17] H. Hübel, A. P. Byrne, S. Ogaza, A. E. Stuchbery, G. D. Dracoulis, and M. Guttormsen, Nucl. Phys. A **453**, 316 (1986).
[18] D. Mehta *et al.*, Z. Phys. A **339**, 317 (1991).
[19] J. J. Lawrie *et al.*, in *Frontiers in Nuclear Structure, Astrophysics, and Reactions: FINUSTAR 3*, 23–27 August 2010, Rhodes, Greece, edited by P. Demetriou, R. Julin, and S. Harissopulos, AIP Conf. Proc. No. 1377 (AIP, New York, 2011), p. 374.
[20] R. T. Newman *et al.*, special issue of Balkan Phys. Lett. **182** (1998).
[21] E. Gueorguieva, M. Kaci, C. Schück, A Minkova, Ch. Vieu, J. J. Correia, J. S. Dionisio, Nucl. Instrum. Methods Phys. Res. A **474**, 132 (2001).
[22] E. Gueorguieva *et al.*, Eur. Phys. J. A **20**, 47 (2004).
[23] E. Gueorguieva *et al.*, iThemba LABS report, 2002 (unpublished).
[24] D. C. Radford, Nucl. Instrum. Methods Phys. Res. A **361**, 297 (1995).
[25] P. L. Masiteng *et al.*, Eur. Phys. J. A **50**, 119 (2014).
[26] G. Duchêne, F. A. Beck, P. J. Twin, G. de France, D. Curien, L. Han, C. W. Beausang, M. A. Bentley, P. J. Nolan, and J. Simpson, Nucl. Instrum. Methods Phys. Res. A **432**, 90 (1999).
[27] H. Helppi, S. K. Saha, P. J. Daly, S. R. Faber, and T. L. Khoo, Phys. Rev. C **28**, 1382 (1983).
[28] A. Görgen *et al.*, Eur. Phys. J. A **6**, 141 (1999).
[29] R. Bengtsson and S. Frauendorf, Nucl. Phys. A **327**, 139 (1979).
[30] W. Nazarewicz, G. A. Leander, and J. Dudek, Nucl. Phys. A **467**, 437 (1985).
[31] J. K. Deng *et al.*, Phys. Lett. B **319**, 63 (1993).